Biomedical Optics EXPRESS

Achromatized endomicroscope objective for optical biopsy

Matthew Kyrish[1] and Tomasz S. Tkaczyk[1,2,*]

[1]*Department of Bioengineering, Rice University, 6100 Main St, Houston, TX 77005, USA*
[2]*Department of Electrical and Computer Engineering, Rice University, 6100 Main St, Houston, TX 77005, USA*
**ttkaczyk@rice.edu*

Abstract: Currently, researchers and clinicians lack achromatized endomicroscope objectives that are as narrow as biopsy needles. We present a proof-of-concept prototype that validates the optical design of an NA0.4 objective. The objective, built with plastic lenses, has a 0.9 mm clear aperture and is achromatized from 452 nm to 623 nm. The objective's measured Strehl ratio is 0.74 ± 0.05 across a 250 μm FOV. We perform optical sectioning via structured illumination through the objective while capturing fluorescence images of breast carcinoma cells stained with proflavine and cresyl violet. This technology has the potential to improve optical biopsies and provide the next step forward in cancer diagnostics.

OCIS codes: (080.3620) Lens system design; (220.0220) Optical design and fabrication; (170.2520) Fluorescence microscopy; (170.3880) Medical and biological imaging; (220.1920) Diamond machining.

References and links

1. National Cancer Institute, "Breast Cancer Risk in American Women," http://www.cancer.gov/cancertopics/factsheet/detection/probability-breast-cancer.
2. Y. Cui, E. A. Koop, P. J. van Diest, R. A. Kandel, and T. E. Rohan, "Nuclear morphometric features in benign breast tissue and risk of subsequent breast cancer," Breast Cancer Res. Treat. **104**(1), 103–107 (2007).
3. L. Mariuzzi, A. Mombello, G. Granchelli, V. Rucco, E. Tarocco, D. Frank, J. Davis, D. Thompson, H. Bartels, G. M. Mariuzzi, and P. H. Bartels, "Quantitative study of breast cancer progression: different pathways for various in situ cancers," Mod. Pathol. **15**(1), 18–25 (2002).
4. T. J. Muldoon, S. Anandasabapathy, D. Maru, and R. Richards-Kortum, "High-resolution imaging in Barrett's esophagus: a novel, low-cost endoscopic microscope," Gastrointest. Endosc. **68**(4), 737–744 (2008).
5. T. J. Muldoon, M. C. Pierce, D. L. Nida, M. D. Williams, A. Gillenwater, and R. Richards-Kortum, "Subcellular-resolution molecular imaging within living tissue by fiber microendoscopy," Opt. Express **15**(25), 16413–16423 (2007).
6. T. J. Muldoon, N. Thekkek, D. Roblyer, D. Maru, N. Harpaz, J. Potack, S. Anandasabapathy, and R. Richards-Kortum, "Evaluation of quantitative image analysis criteria for the high-resolution microendoscopic detection of neoplasia in Barrett's esophagus," J. Biomed. Opt. **15**(2), 026027 (2010).
7. S. M. Landau, C. Liang, R. T. Kester, T. S. Tkaczyk, and M. R. Descour, "Design and evaluation of an ultra-slim objective for *in-vivo* deep optical biopsy," Opt. Express **18**(5), 4758–4775 (2010).
8. T. Tot and L. Tabár, "The role of radiological-pathological correlation in diagnosing early breast cancer: the pathologist's perspective," Virchows Arch. **458**(2), 125–131 (2011).
9. J. C. Jung and M. J. Schnitzer, "Multiphoton endoscopy," Opt. Lett. **28**(11), 902–904 (2003).
10. P. Kim, M. Puoris'haag, D. Côté, C. P. Lin, and S. H. Yun, "*In vivo* confocal and multiphoton microendoscopy," J. Biomed. Opt. **13**(1), 010501 (2008).
11. Y. Zhao, H. Nakamura, and R. J. Gordon, "Development of a versatile two-photon endoscope for biological imaging," Biomed. Opt. Express **1**(4), 1159–1172 (2010).
12. Y. Wu and X. Li, "Combined influences of chromatic aberration and scattering in depth-resolved two-photon fluorescence endospectroscopy," Biomed. Opt. Express **1**(4), 1234–1243 (2010).
13. GRINTECH GmbH, "GRIN lens systems for medical applications," http://www.grintech.de/grin-lens-systems-for-medical-applications.html.
14. D. C. Leiner and R. Prescott, "Correction of chromatic aberrations in GRIN endoscopes," Appl. Opt. **22**(3), 383–386 (1983).
15. M. T. Myaing, D. J. MacDonald, and X. Li, "Fiber-optic scanning two-photon fluorescence endoscope," Opt. Lett. **31**(8), 1076–1078 (2006).

#179669 - $15.00 USD Received 13 Nov 2012; revised 9 Jan 2013; accepted 18 Jan 2013; published 18 Jan 2013

16. T. H. Chia and M. J. Levene, "Microprisms for *in vivo* multilayer cortical imaging," J. Neurophysiol. **102**(2), 1310–1314 (2009).
17. R. T. Kester, T. Christenson, R. R. Kortum, and T. S. Tkaczyk, "Low cost, high performance, self-aligning miniature optical systems," Appl. Opt. **48**(18), 3375–3384 (2009).
18. M. D. Chidley, K. D. Carlson, R. R. Richards-Kortum, and M. R. Descour, "Design, assembly, and optical bench testing of a high-numerical-aperture miniature injection-molded objective for fiber-optic confocal reflectance microscopy," Appl. Opt. **45**(11), 2545–2554 (2006).
19. K.-B. Sung, C. Liang, M. Descour, T. Collier, M. Follen, and R. Richards-Kortum, "Fiber-optic confocal reflectance microscope with miniature objective for *in vivo* imaging of human tissues," IEEE Trans. Biomed. Eng. **49**(10), 1168–1172 (2002).
20. E. Laemmel, M. Genet, G. Le Goualher, A. Perchant, J.-F. Le Gargasson, and E. Vicaut, "Fibered confocal fluorescence microscopy (Cell-viZio) facilitates extended imaging in the field of microcirculation. A comparison with intravital microscopy," J. Vasc. Res. **41**(5), 400–411 (2004).
21. A. Osdoit, M. Genet, A. Perchant, S. Loiseau, B. Abrat, and F. Lacombe, "*In vivo* fibered confocal reflectance imaging: totally non-invasive morphological cellular imaging brought to the endoscopist," Proc. SPIE **6082**, 608208, 608208-10 (2006).
22. A. R. Rouse, A. Kano, J. A. Udovich, S. M. Kroto, and A. F. Gmitro, "Design and demonstration of a miniature catheter for a confocal microendoscope," Appl. Opt. **43**(31), 5763–5771 (2004).
23. A. R. Tumlinson, B. Povazay, L. P. Hariri, J. McNally, A. Unterhuber, B. Hermann, H. Sattmann, W. Drexler, and J. K. Barton, "*In vivo* ultrahigh-resolution optical coherence tomography of mouse colon with an achromatized endoscope," J. Biomed. Opt. **11**(6), 064003 (2006).
24. D. Wang, B. V. Hunter, M. J. Cobb, and X. Li, "Super-achromatic rapid scanning microendoscope for ultrahigh-resolution OCT imaging," IEEE J. Sel. Top. Quantum Electron. **13**(6), 1596–1601 (2007).
25. G. C. Birch, M. R. Descour, and T. S. Tkaczyk, "Hyperspectral Shack-Hartmann test," Appl. Opt. **49**(28), 5399–5406 (2010).
26. G. I. Greisukh, E. G. Ezhov, I. A. Levin, and S. A. Stepanov, "Design of achromatic and apochromatic plastic micro-objectives," Appl. Opt. **49**(23), 4379–4384 (2010).
27. N. Bozinovic, C. Ventalon, T. Ford, and J. Mertz, "Fluorescence endomicroscopy with structured illumination," Opt. Express **16**(11), 8016–8025 (2008).
28. J. Bini, J. Spain, K. Nehal, V. Hazelwood, C. DiMarzio, and M. Rajadhyaksha, "Confocal mosaicing microscopy of human skin *ex vivo*: spectral analysis for digital staining to simulate histology-like appearance," J. Biomed. Opt. **16**(7), 076008 (2011).
29. D. S. Gareau, "Feasibility of digitally stained multimodal confocal mosaics to simulate histopathology," J. Biomed. Opt. **14**(3), 034050 (2009).
30. W. Göbel, D. Brucker, Y. Kienast, A. Johansson, G. Kniebühler, A. Rühm, S. Eigenbrod, S. Fischer, M. Goetz, F.-W. Kreth, A. Ehrhardt, H. Stepp, K.-M. Irion, and J. Herms, "Optical needle endoscope for safe and precise stereotactically guided biopsy sampling in neurosurgery," Opt. Express **20**(24), 26117–26126 (2012).
31. M. Kyrish, U. Utzinger, M. R. Descour, B. K. Baggett, and T. S. Tkaczyk, "Ultra-slim plastic endomicroscope objective for non-linear microscopy," Opt. Express **19**(8), 7603–7615 (2011).
32. B. McCall, M. Pierce, E. A. Graviss, R. Richards-Kortum, and T. Tkaczyk, "Toward a low-cost compact array microscopy platform for detection of tuberculosis," Tuberculosis (Edinb.) **91**(Suppl 1), S54–S60 (2011).
33. T. S. Tkaczyk, J. D. Rogers, M. Rahman, T. C. Christenson, S. Gaalema, E. L. Dereniak, R. Richards-Kortum, and M. R. Descour, "Multi-modal miniature microscope: 4M Device for bio-imaging applications - an overview of the system," Proc. SPIE **5959**, 59590N, 59590N-9 (2005).
34. S. Bäumer, *Handbook of Plastic Optics* (Wiley, 2011).
35. ISO, "Photography—electronic still-picture cameras—resolution measurements," ISO 12233:2000, http://www.iso.org/iso/home/store/catalogue_tc/catalogue_detail.htm?csnumber=33715.

1. Introduction

Breast cancer is a disease that will affect one in eight women in America during their lifetime [1]. When a suspicious region of the breast is identified during screening, usually via mammogram or clinical breast exam, a diagnosis is needed. Diagnoses typically require removing tissue samples or cells via invasive biopsy before a pathologist examines them with a bench top microscope. Cellular organization and nuclear size and shape are used to identify benign tissue, carcinoma *in situ*, invasive cancer, and other types of tissue, including inflammation and atypical hyperplasia [2,3]. A potential alternative to conventional biopsies is an "optical biopsy," which uses a needle-sized endomicroscope to provide real-time, *in vivo* microscopy images without tissue removal. The endomicroscope can pierce the tissue to the region of interest, like a conventional biopsy needle, and then relay microscopic images out of the patient, allowing a mid-biopsy diagnosis. Optical biopsies should provide similar results to the current gold standard for diagnosis: conventional biopsy followed by H&E histology

#179669 - $15.00 USD Received 13 Nov 2012; revised 9 Jan 2013; accepted 18 Jan 2013; published 18 Jan 2013

staining. Therefore, endomicroscopes should have sub-cellular resolution, optical sectioning capability, and the ability to image multiple dyes simultaneously. We are developing an endomicroscope objective that fulfills these three conditions.

Current endomicroscopes may use a fiber bundle, also called an image guide, to relay light from the region of interest to the imaging system without using an objective at the distal tip. A high-resolution microendoscope (HRME) has successfully imaged subcellular features and tissue organization in the oral cavity using a probe approximately 1 mm wide [4–6]. Because the outer diameter (OD) of core biopsies needles is 0.9 mm to 2.1 mm, this endomicroscope is narrow enough to perform an optical biopsy. After staining the tissue with proflavine, a fluorescent dye, the HRME displays the nuclei in the oral cavity as bright ovals. However, although the nuclei can be seen with the HRME, they cannot be sufficiently resolved, particularly in breast tissue. The nuclear diameter is approximately 5-10 μm, while the current resolution of the HRME is 8 μm, due to the fibers' core-to-core spacing of 4 μm. Landau et al. [7] added a 3.2X objective to the tip of the same coherent fiber bundle, providing a resolution of 2.5 μm. A system with higher resolution would improve clinicians' ability to identify cellular atypia, the absence of a myoepithelial cell layer, and invasion of cancer cells into normal tissue, all of which indicate malignancy [8]. This objective, like the one reported by Landau et al. [7], will help achieve this higher resolution.

Some endomicroscopes use gradient index (GRIN) lenses as objectives at their distal tip. GRIN lenses are glass cylinders with a quadratically varying index of refraction along their radius. They suffer from strong spherical and chromatic aberrations [9–12]. When combined with a refractive glass lens, GRIN lenses can form objectives with limited monochromatic aberration correction and increased NA [13] while maintaining outer diameters as small as or smaller than a biopsy needle [14–16]. However, without axial chromatic aberration correction in the imaging system, dyes with different emission spectra cannot be imaged without one or more appearing blurred.

Other miniature objectives utilizing conventional refractive lenses have also been designed and tested [17–24]. In all cases, the OD of the objective was significantly larger than the OD of a core biopsy needle (their diameters were between 2.6 mm and 7 mm) or the objective was designed for a single wavelength. Although others have recognized the advantages offered by plastic lenses and proposed achromatized systems [25,26], no one has yet constructed such devices, to the best of our knowledge. Our plastic lens objective is achromatized and the clear aperture is 0.9 mm, which can allow the distal optics to remain as narrow as a biopsy needle.

To perform *in vivo* optical biopsies of thick tissue with high contrast images, optical sectioning is required to image a thin tissue slice and reject background light. Optical sectioning can be achieved via confocal, structured illumination, or multiphoton fluorescence imaging. The achromatic objective we are developing will be part of an endomicroscope which utilizes structured illumination, similar to that reported by Bozinovic et al. [27].

Recently, several papers showed the promising trend of mimicking H&E staining by creating pseudocolor images of excised tissue captured with fluorescence and reflectance confocal microscopy [28,29]. Göbel et al. also presented an optical biopsy system utilizing a fiber bundle without a distal objective which is capable of capturing *in vivo* fluorescence images of endogenous and exogenous sources [30]. Such images may help in pathological assessment. In the future, we will pursue real-time *in vivo* pseudocolor imaging of breast tissue by using multiple fluorescent dyes which target the nucleus and the cytoplasm. To perform this imaging *in vivo*, we require an endomicroscope utilizing an achromatized objective lens.

In this study, we present a prototype which validates the optical design of an achromatized objective. The proof-of-concept demonstrates the ability to create an achromatized objective composed only of plastic lenses with a clear aperture of 0.9 mm and NA = 0.4. Although the current prototype is built in large discs, future iterations may be integrated into hypodermic

#179669 - $15.00 USD Received 13 Nov 2012; revised 9 Jan 2013; accepted 18 Jan 2013; published 18 Jan 2013

tubes, using previously described techniques [17,31], and then incorporated into endomicroscopes.

2. Design

The ultra-slim, all-plastic objective has been designed to achieve diffraction limited performance across a 171 nm wavelength range within the visible spectrum following the specifications listed in Table 1. The objective is particularly designed to work with two fluorescent dyes, proflavine and cresyl violet, which inherently stain the nucleus and cytoplasm, respectively. Proflavine has excitation and emission peaks at 452 nm and 515 nm. Cresyl violet has excitation and emission peaks at 575 nm and 623 nm.

Table 1. Achromatic ultra-slim objective design specifications

Object Space NA[a]	0.4
Image Space NA	0.14
Field of View (FOV)	250 μm
Clear Aperture	0.9 mm
Magnification	–2.88
Working Distance[a]	15 μm
Wavelength Range	452-623 nm
Telecentricity	Object Space

[a]Object space is intended for water immersion.

At the center wavelength of 538 nm, an NA0.4 objective provides a diffraction limited resolution of 0.82 μm. A 0.9 mm clear aperture will allow the objective to be integrated with an endomicroscope to perform optical biopsies. The magnification matches the 250 μm FOV to the 720 μm imaging area of the endomicroscope's fiber bundle. The short, 15 μm working distance allows the objective to image tissue while in direct contact. This distance can be increased for different applications by re-optimizing the design; for instance, our NA0.4 ultra-slim objective for non-linear imaging has a working distance of 200 μm [31]. Telecentricity is maintained in object space. We previously reported that achieving image space telecentricity would mean compromising transverse magnification and performance at the edge of the image [7]. To counteract this effect, the principal ray angle was allowed to deviate from 0°. The analysis shows that, while this created some vignetting, the image quality is higher than if the design were strictly image space telecentric.

The justification for using plastic as a lens material, particularly during fluorescence imaging, has already been detailed [31,32]. To summarize, the first and last lenses are composed of Zeonex E48R due to its crown-like optical properties and very low water absorption. Both doublets are made of PMMA, NOA61, and polystyrene. PMMA is a crown-like plastic while polystyrene behaves like a flint, allowing achromatization. The plastics have high transmission and negligible autofluorescence across the design wavelength range. Creating aspheres in plastic lenses is no different from creating spheric surfaces, allowing simpler, cheaper designs using fewer components than glass.

A lens prescription meeting the design requirements was developed in Zemax and is listed in Table 2. The objective design layout is illustrated in Fig. 1 and the nominal performance is shown in Fig. 2. Figure 2(a) plots the polychromatic MTF of the achromatic objective; it has diffraction limited performance except for the sagittal ray at edge of the FOV for polychromatic light. Figure 2(b) shows the image space chromatic focal shift; the maximum shift, 3.2 μm, is much shorter than the diffraction limited range of 22.0 μm. For this particular lens system, the expected transmission efficiency based on the Fresnel equations and the transmission rates measured in Kyrish et al. [31] is 58%; however, Tkaczyk et al. [33] created a significant improvement in their microscope's throughput by adding AR coatings to the plastic lenses. This procedure can be used in future implementations to improve the transmission efficiency of the achromatic objective.

#179669 - $15.00 USD Received 13 Nov 2012; revised 9 Jan 2013; accepted 18 Jan 2013; published 18 Jan 2013

Table 2. Lens prescription of the achromatic objective

Notes	Radius (mm)	Thickness (mm)	Glass	4th Order Aspheric Term	6th Order Aspheric Term	8th Order Aspheric Term
Object	1.50000	0.046	Seawater			
Lens 1	–0.29789	1.000	E48R			
	–0.62850	0.025				
Lens 2	1.13232	1.070	PMMA	–0.095743	0.579417	–1.044467
	–0.59716	0.050	NOA61			
Lens 3	–0.54874	1.000	Polystyrene			
	–2.26094	0.000		–0.093718	0.831976	–3.102985
Stop	Infinity	0.050				
Lens 4	1.35360	1.080	PMMA	–0.048849	–0.026626	
	–0.78475	0.050	NOA61			
Lens 5	–0.79370	2.012	Polystyrene			
	–1.00743	0.025		0.392702	–0.165720	0.183568
Lens 6	–2.31762	1.000	E48R			
	1.16361	0.286		–0.860845		
Image	Infinity					

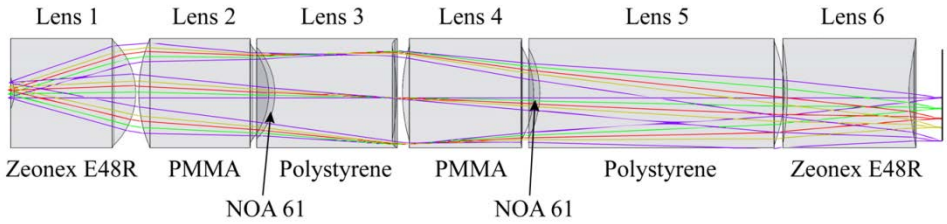

Fig. 1. Schematic representation of the achromatic objective. The diameter of the lenses is 0.9 mm.

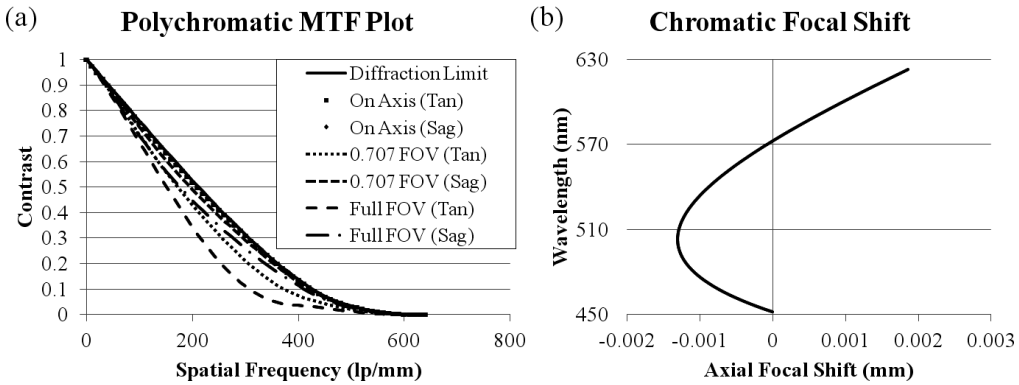

Fig. 2. Nominal performance of the achromatic objective. (a) Diffraction limited polychromatic MTF. (b) Diffraction limited image space chromatic focal shift.

A thorough tolerancing of the design was also performed in Zemax. The tolerances listed in Table 3 are based on in-house fabrication capabilities. The lenses were formed via single point diamond turning (SPDT) using an ultra-precision lathe. Injection molding can be used to mass produce the lenses; for injection molding, the tolerances are considered commercial or state-of-the-art [34].

#179669 - $15.00 USD Received 13 Nov 2012; revised 9 Jan 2013; accepted 18 Jan 2013; published 18 Jan 2013

Table 3. Tolerancing of the achromatic objective

Tolerand	Value
Radius of curvature (%)	±1
Thickness (μm)	±20
Element decenter (μm)	±10
Element tilt (°)	±0.15
Doublet decenter (μm)	±15
Doublet tilt (°)	±0.2
Surface irregularity (fringes)	±1
Index (%)	±1
Abbe Number (%)	±1

3. Fabrication and assembly

A design proof-of-principle prototype of the ultra-slim achromatic objective was built in 22 mm diameter plastic disks; while too large to be used in an endomicroscope, this allows the optical design to be validated. The fabrication process is similar to that described by McCall et al. [32]; using SPDT, the optical surfaces and the optomechanics were cut into the plastic disks, creating positive and negative alignment features in the same material as the lenses. Using the ultra-precision lathe to simultaneously create the optics and the mechanics maintains tight tolerances for radius, thickness, decentration, tilt, and surface irregularity. The objective was modeled in SolidWorks; a cutaway view is shown in Fig. 3(a). The positive annular features on the bottom of each lens are designed to be concentric with the negative triangular features of the following lens at two points. Blue permanent marker is added 5 mm away from the optical axis up to the edge of the clear aperture of each optical surface, creating baffles within the objective. These baffles reduce stray light, maintaining high contrast. Cemented doublets are held together by applying NOA61 directly to the concave optical surface. The lenses are stacked, two at a time, while mating the positive and negative alignment features. This procedure centers the lenses and ensures the designed spacing within the optical system. The adhesive is then cured with ultraviolet light. For the remaining lenses, a small amount of glue is added to the grooves and the edge of the discs before stacking the components. Figure 3(b) shows lenses 2 and 3 from Fig. 1 next to a US quarter. Figure 3(c) presents a fully assembled achromatic objective. In the future, this design will be built within a 1.4 mm OD hypodermic tube, as we have demonstrated before [31].

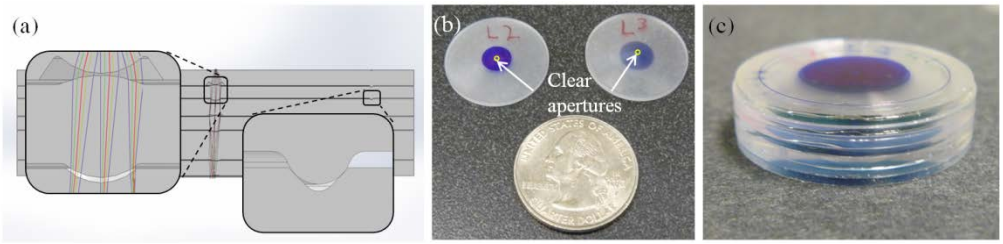

Fig. 3. (a) SolidWorks cutaway of the assembled achromatic objective with built-in alignment features used to validate the optical design. The insets show optical surfaces (left) and alignment features (right). (b) Example of two singlet lenses next to a US quarter with the clear apertures of the lenses circled. (c) Fully assembled prototype achromatic objective.

4. Characterization and testing

The functionality and performance of the achromatic objective were thoroughly characterized. First, doublet lenses were cut and assembled in order to measure their tilt and decentration. Next, the lateral performance and chromatic focal shift of a fully assembled objective were measured. Finally, the objective was used to image breast carcinoma cells which were stained with multiple fluorescent dyes. In order to demonstrate the limitations of a monochromatic objective and the need for achromatization, the chromatic focal shift measurement and

#179669 - $15.00 USD Received 13 Nov 2012; revised 9 Jan 2013; accepted 18 Jan 2013; published 18 Jan 2013

fluorescence imaging were also performed on a monochromatic objective prototype previously described by Landau et al. [7].

Copies of lens 2 and lens 3 (Fig. 3(b)) were fabricated and assembled to measure the tilt and decentration of the doublets. The doublet's tilt was measured with a NewView 5020 white light interferometer (Zygo). The doublet was placed on a microscope slide with its tilt reduced to less than 0.007° by adjusting the tilt of the interferometer's stage until the total runout was less than 1 μm over an area of 7.25 mm x 5.44 mm (Fig. 4(a)). Then the doublet's tilt was measured 5 times on each side. The average tilt was 0.093° with a standard deviation of 0.055°, indicating that the tilt is within tolerance. The decenter was measured using the integrated gage amplifier (IGA) of an ultra-precision lathe (Precitech). One lens of the doublet was centered on the spindle of the machine within 2 μm using the IGA (Fig. 4(b)). Then the runout of the second lens was measured. Any increase in runout corresponds to a decenter of half that value. This measurement was performed 5 times for each singlet. The average element decenter of the doublet was 6.1 μm with a standard deviation of 0.7 μm, again indicating that doublets can be built with acceptable deviations from nominal.

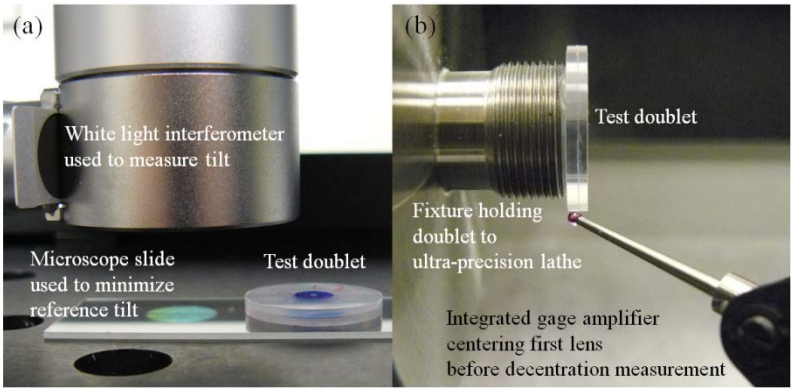

Fig. 4. (a) Measuring tilt with a white light interferometer. The doublet's average tilt was 0.093° with a standard deviation of 0.055°. (b) Measuring decenter with an integrated gage amplifier. The doublet's average decenter was 6.1 μm with a standard deviation of 0.7 μm.

To measure the lateral, polychromatic resolution of the achromatic objective, an image of a hi-resolution target was relayed in reverse (placing the target in the image space of the achromatic objective). This setup causes the resolution to be limited by the achromatic objective's image space NA = 0.14. For NA0.14, the Rayleigh resolution limit in white light is 2.40 μm, or 417 lp/mm, assuming a central wavelength of 550 nm. The hi-resolution target has features up to 645 lp/mm, so the target can be used to assess the smallest features the objective can resolve. The custom objective was set up to relay an image through an inverted microscope (Zeiss Axio Observer. A1, Zeiss) under white light trans-illumination. The object is placed in image space and a 40X, NA0.75 water immersion commercial objective (Zeiss) relays an image through the microscope to a CCD camera (Fig. 5(a)). The results are seen in Fig. 6(a) and Fig. 6(b). Because the custom objective is designed for a curved object (acceptable for imaging thick tissue), there is some field curvature and loss of performance at the edge of the FOV while imaging flat objects. The qualitative performance of the system was determined by locating the smallest resolvable feature, in this case group 8, element 5, which is 406 lp/mm. This is close to the theoretical diffraction limit, 417 lp/mm and is similar to the monochromatic performance of the objective described by Landau et al. [7].

The achromatic objective's performance was further analyzed by measuring the Strehl ratio via the slanted-edge method of calculating the MTF [18]. An edge object was placed in front of the system in water immersion and the image was relayed with a 10X, NA0.3 Plan-Neofluar objective (Zeiss) (Fig. 5(b)). A VariSpec liquid crystal tunable filter (LCTF) (CRi)

#179669 - $15.00 USD Received 13 Nov 2012; revised 9 Jan 2013; accepted 18 Jan 2013; published 18 Jan 2013

filtered the light to match the four design wavelengths (452 nm, 515 nm, 575 nm, and 623 nm); the LCTF creates ~10 nm wide bands. For each waveband, sixteen edges were inspected, eight near the center and eight near 50% of the FOV. Figure 6(c) shows a set of four measured edges from one corner of a square on the resolution target; the remaining twelve edges were obtained from the square's three other corners. An MTF curve was generated from each edge

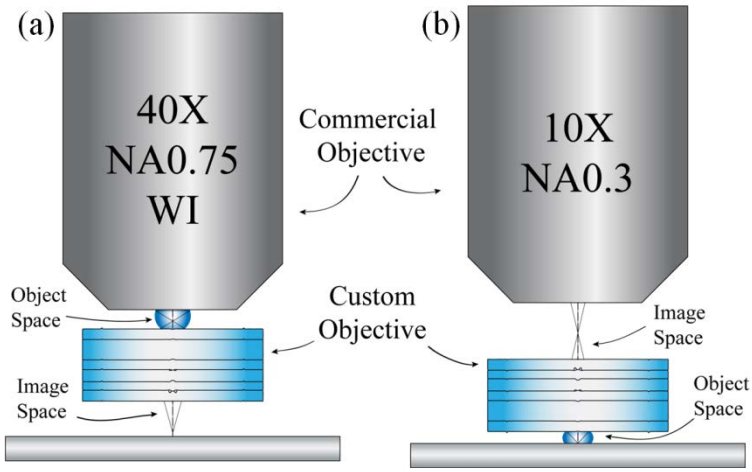

Fig. 5. Custom achromatic objective and commercial Zeiss objectives (a) relaying images in reverse and (b) relaying images as designed.

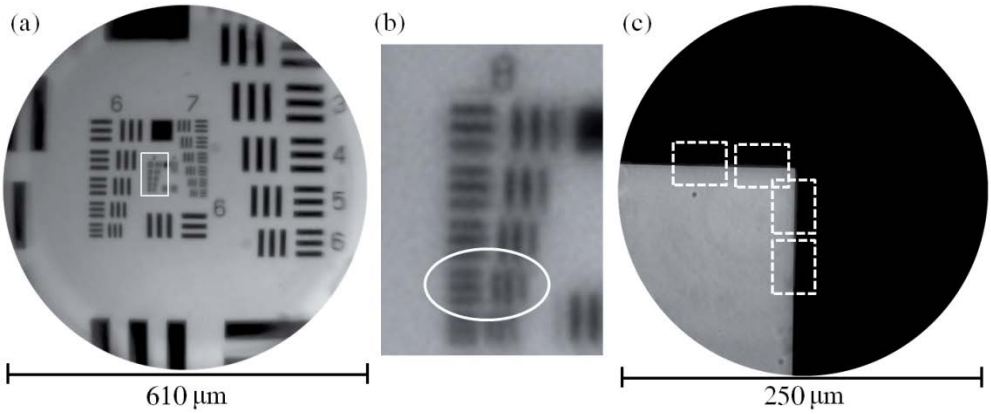

Fig. 6. (a) The center of a hi-resolution 1951 USAF target illuminated with white light in transmission. The achromatic objective is operating in reverse, which means the resolution is limited by the image space NA = 0.14. (b) The region of interest outlined in (a). The smallest resolvable feature is group 8, element 5, which has a spatial frequency of 406 lp/mm. The theoretical diffraction limit is 417 lp/mm. (c) Set of four edges measured with the slanted edge method to determine the achromatic objective's MTF and Strehl ratio.

using the ISO 12233 standard [35]. The polychromatic MTF curve was created by averaging all 64 narrowband curves and is displayed in Fig. 7(a) compared to the diffraction limit. The Strehl ratio is 0.74 ± 0.05.

The chromatic focal shifts of both the achromatic objective and the monochromatic objective described by Landau et al. [7] were measured using an MT25 precision length gauge (Heidenhain) to record the axial position of the stage. The LCTF was set to 450 nm and the best focal plane was found. The LCTF's wavelength was increased by 20 nm and the new best focal plane was measured. This process was repeated until the wavelength reached 630 nm. The procedure was performed five times for each prototype objective, and the relative shifts

#179669 - $15.00 USD Received 13 Nov 2012; revised 9 Jan 2013; accepted 18 Jan 2013; published 18 Jan 2013

were averaged to find the chromatic focal shifts of the objectives, which are plotted in Fig. 7(b) alongside the nominal shifts. The achromatic objective successfully brings two wavelengths of light into focus simultaneously while the monochromatic objective does not. Also, although the measured shifts were larger than expected, the achromatic objective's 11.4 μm maximum focal shift is smaller than the diffraction limited focal range of 22.0 μm. In contrast, the monochromatic objective's 196.4 μm shift is almost an order of magnitude

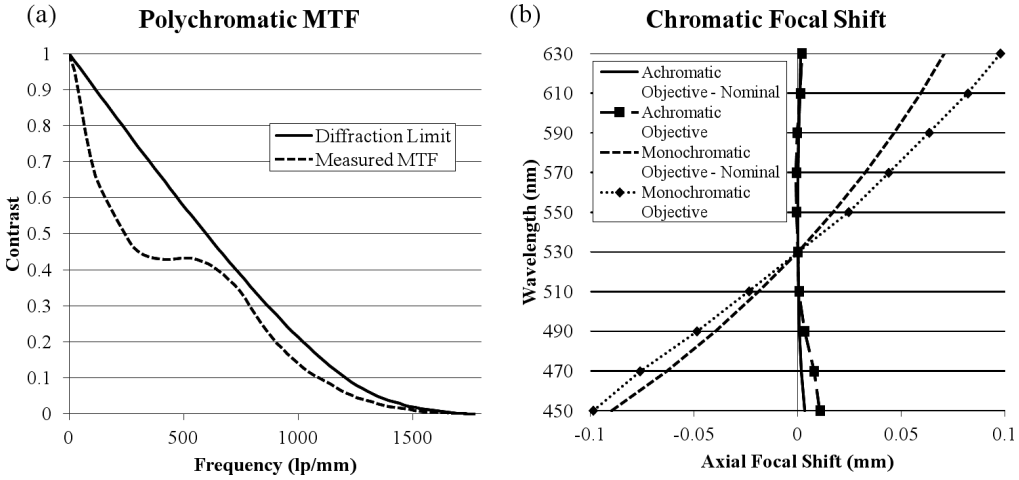

Fig. 7. (a) Polychromatic MTF of the achromatic objective. (b) Chromatic focal shifts of the achromatic objective and the monochromatic objective.

greater than the diffraction limited focal range. To the best of our knowledge, we have built the first all plastic, achromatic microscope objective.

5. Imaging results

In vitro breast carcinoma cells from the 435S cell line were used for biological imaging with both prototype objectives. The cells were seeded on an 8-well microscope slide and stained with proflavine and cresyl violet. The proflavine, or 3,6-diaminoacridine hydrochloride (Sigma), was prepared as a 0.025% weight volume solution in 1X phosphate buffered saline (PBS) (Sigma), while the cresyl violet (Sigma) was prepared as a 0.05% weight volume solution in 1X PBS. Two hundred μL of each fluorescent dye solution were added to each well. The cells were stained for 5 minutes before the dye was removed. Each chamber was then washed with 500 μL of 1X PBS to remove excess dye.

The breast carcinoma cells were imaged with the monochromatic and achromatic objectives separately through the Zeiss Imager.Z1, as well as with a Zeiss NA0.45 commercial objective. Using a GFP filter set, proflavine was excited without exciting cresyl violet. The cells were brought into focus and an image was captured with the Imager's monochrome camera. Without adjusting the position of the stage, we then imaged cresyl violet through a Texas Red filter set. The separate proflavine and cresyl violet images were recombined into single, pseudocolor images (Fig. 8). The Zeiss objective (Fig. 8, top row) demonstrates that proflavine preferentially stains nuclei while cresyl violet is concentrated in the cytoplasm. Both the monochromatic and achromatic objectives clearly showed proflavine staining the nucleus (Fig. 8, left column). However, the cytoplasm is blurry at the red wavelength when the cells are imaged with the monochromatic objective (Fig. 8, center).

The cells were also imaged using structured illumination via the ApoTome attachment to the Imager.Z1 microscope using the procedure described above. Because the cells were already a monolayer, there was only a modest contrast improvement; when optically sectioning thick tissue, the reduction in background fluorescence will create a greater increase

#179669 - $15.00 USD Received 13 Nov 2012; revised 9 Jan 2013; accepted 18 Jan 2013; published 18 Jan 2013

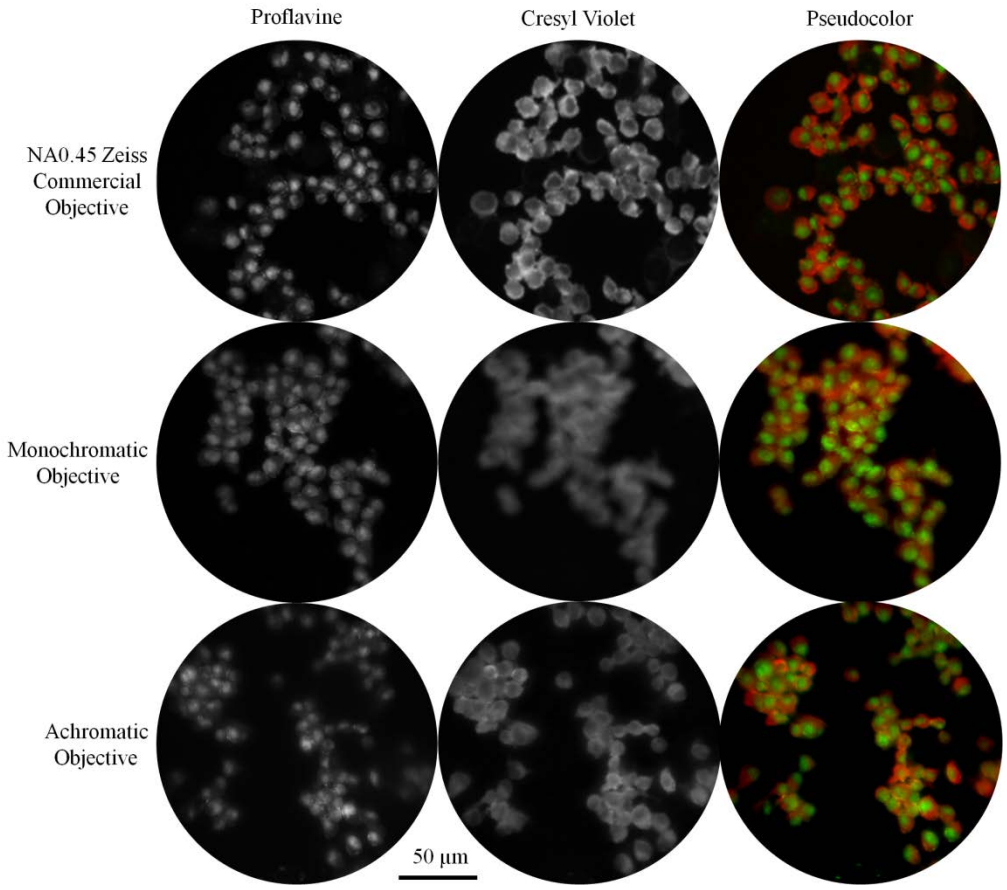

Fig. 8. Images of cells from the 435S breast carcinoma cell line stained with proflavine and cresyl violet. The commercial Zeiss objective and the prototype achromatic objective provide high resolution images for proflavine and cresyl violet simultaneously. In contrast, cresyl violet is out of focus with the monochromatic objective.

in contrast. The commercial objective and achromatic objective again provided high quality images for both fluorescent dyes, while the monochromatic objective lost performance when imaging cresyl violet (Fig. 9). There is also a loss of intensity due to the structured illumination grid pattern being focused at a different depth. These effects are due to chromatic aberration; the focal planes for the excitation and emission wavelengths, which are conjugate for the commercial and achromatic objectives, are separated with the monochromatic objective.

#179669 - $15.00 USD Received 13 Nov 2012; revised 9 Jan 2013; accepted 18 Jan 2013; published 18 Jan 2013

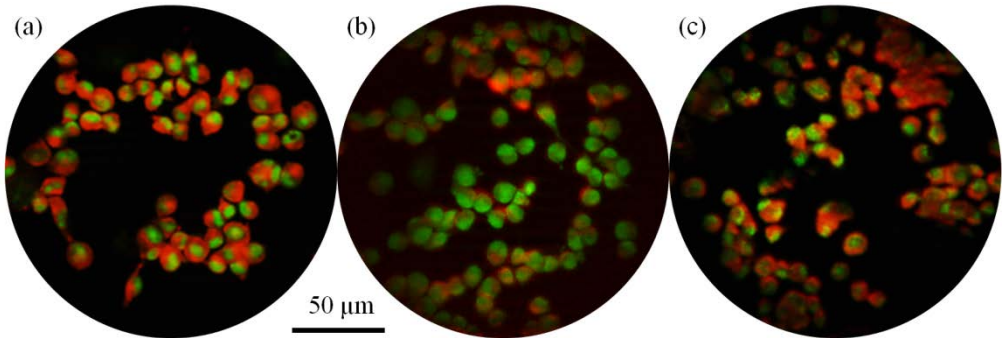

Fig. 9. Structured illumination images of cells from the 435S breast carcinoma cell line stained with proflavine and cresyl violet. Structured illumination was created with the Zeiss ApoTome and the cells were imaged with (a) the NA0.45 Zeiss commercial objective, (b) the monochromatic objective, and (c) the achromatic objective.

6. Conclusion

An all-plastic, achromatic objective has been designed, toleranced, fabricated, and tested. The NA0.4 objective is an alternative to GRIN lenses, which suffer from significant chromatic aberration as well as performance loss across the FOV. Our objective is achromatized and maintains its performance across the designed 250 µm FOV, achieving a Strehl ratio of 0.74 ± 0.05 while holding the optical surfaces' clear apertures to 0.9 mm. Wide-field fluorescence imaging and optical sectioning via structured illumination are performed through the achromatic objective. Background reduction, via optical sectioning or another method, is critical when fluorescently imaging dense samples like breast tissue; without such methods, high levels of background create low contrast images. The achromatic objective permits using multiple dyes simultaneously, allowing staining which more closely mimics conventional histology. An ultra-slim achromatic objective can bring clinicians one step closer to performing high resolution, high contrast, *in vivo* optical biopsies to provide reliable cancer diagnoses.

Acknowledgments

We thank Vivian Mack for breast carcinoma cell preparation and Michal Pawlowski, Brian McCall, and Richard Schwarz for comments on the manuscript. Funding was provided by NIH grants R01 EB007594 and R01 CA124319.